1993ApJ...417..259F

THE ASTROPHYSICAL JOURNAL, 417:259–264, 1993 November 1
© 1993. The American Astronomical Society. All rights reserved. Printed in U.S.A.

INITIAL WHITE DWARF RESULTS FROM THE *EXTREME ULTRAVIOLET EXPLORER*

DAVID S. FINLEY, PATRICK JELINSKY, AND JEAN DUPUIS
Center for EUV Astrophysics, 2150 Kittredge Street, University of California, Berkeley, CA 94720
AND
DETLEV KOESTER
Department of Physics and Astronomy, Louisiana State University, Baton Rouge, LA 70803-4001
Received 1993 March 30; accepted 1993 May 7

ABSTRACT

The *Extreme Ultraviolet Explorer* satellite (*EUVE*), which completed its all-sky photometric survey in 1993 January, is providing a wealth of new data for a variety of astrophysically interesting objects, from planets to active galaxies. The wavelength coverage provided by *EUVE*, 50–740 Å, comprises nearly the full range of the extreme ultraviolet (EUV). For hot white dwarfs, the EUV data are useful for constraining the temperatures, trace element abundances, and interstellar columns. The objects selected for this initial analysis are three nearby (<60 pc) hot DA white dwarfs, previously observed in the EUV, and apparently possessing pure hydrogen atmospheres. We present our results, of stellar properties and ISM columns for these three white dwarfs, and discuss the implications for the characteristics of the white dwarfs and the state of the local ISM. We also compare our results with those based on previous observations as a check of the relative calibrations of the different instruments.

Subject headings: ISM: abundances — ultraviolet: stars — white dwarfs

1. INTRODUCTION

Extreme ultraviolet (EUV) measurements are an essential part of the multiwavelength observational approach that is necessary for a full characterization of the properties of hot DA white dwarfs. EUV observations have been providing important results since HZ 43 was detected as the first extrasolar EUV source (Lampton et al. 1976). That observation fostered the realization that hot white dwarfs can be copious EUV emitters, with emergent fluxes in the EUV exceeding that of a blackbody of the same effective temperature by orders of magnitude (Shipman 1979). Subsequent EUV observations with *Einstein*, *EXOSAT*, and *ROSAT* have played a key role in demonstrating that DA white dwarfs are not monoelemental, as they usually appear in the optical, with many of the hotter ($T_{\rm eff} > 40{,}000$ K) DAs having significantly diminished EUV fluxes due to the presence of trace absorbers in their photospheres (Kahn et al. 1984; Jordan et al. 1987; Paerels & Heise 1989; Barstow et al. 1993). The analysis of these observations and discussion of the theoretical implications have been the subject of papers which are too numerous to summarize here. A recent review of the subject of trace elements in DA white dwarfs may be found in Vennes, Thejll, & Shipman (1991).

2. *EUVE* MISSION AND INSTRUMENTATION

For a more complete description of the *Extreme Ultraviolet Explorer* (*EUVE*) instruments and the *EUVE* mission, we refer the reader to Bowyer & Malina (1991). In short, the primary mission of *EUVE* is the performance of a 6 month all-sky survey, which was carried out by the three coaligned scanning telescopes following the initial commissioning phase. The scanning telescopes have fixed, segmented thin-film filters attached to the detectors which define four different bandpasses spanning the range of 50–740 Å. As the spacecraft spun during the survey, the filters provided either simultaneous or nearly simultaneous measurements in the different bandpasses. The fourth instrument, the Deep Survey/Spectrometer, is oriented orthogonally to the scanner telescopes and provided a very sensitive deep survey along a 2° wide swath along half the ecliptic plane. That instrument also includes a three-channel spectrometer, which is being used for pointed spectroscopic observations in the period following the completion of the sky survey. Each instrument consists of a grazing incidence telescope that focuses radiation onto an imaging, photon-counting microchannel plate detector.

The different photometers and their bandpasses are listed in Table 1 (limits are defined as the wavelengths at which the effective area is 10% of the peak value). *EUVE* is performing the first full sky survey in the bandpasses longward of Lexan, and many objects are being detected even in the two longest wavelength bandpasses. (While *EXOSAT* had an Al/Parylene bandpass equivalent to our Al/C bandpasses, it operated in pointed mode only, and only about 20 white dwarfs were observed and detected.) The advantages of *EUVE*'s full wavelength coverage for white dwarfs include an improved capability for separating the effects of photospheric composition and interstellar column, and the ability to determine H I and He I columns separately for objects detected in the two long-wavelength filters, which cover either side of the He I 504 Å edge.

3. INITIAL OBSERVATIONS OF WHITE DWARFS

White dwarf observations are critical to our performance verification and sensitivity monitoring program for *EUVE*. White dwarfs were observed in pointed mode for calibration purposes prior to the start of the survey and during the survey, and the same objects are also being reobserved during the subsequent phase of spectroscopic observations, providing an extended baseline for monitoring any changes in sensitivity during the course of the mission. By observing white dwarfs with different temperatures and columns, we are obtaining data from objects with a range of continuum flux distributions with which to evaluate the calibration as a function of wavelength. This evaluation is facilitated by our ability to model the

© American Astronomical Society • Provided by the NASA Astrophysics Data System

1993ApJ...417..259F

TABLE 1

EUVE CORRECTED COUNT RATES

Instrument	Range (Å)	WD 0050−332	WD 1620−391	WD 1845+019
Scanner Lexan/B	50–180	1.78 (0.018)	...	...
Scanner Al/C/Ti	160–240	0.86 (0.013)	...	...
Scanner Ti/Sb/Ti/Al	345–605	<0.0016	<0.01	...
Scanner Sn/SiO	500–740	<0.0036	<0.02	...
Deep Survey Lexan/B	65–190	...	0.96 (0.007)	1.44 (0.007)
Deep Survey Al/C	160–360	...	0.25 (0.016)	1.12 (0.02)

flux from the white dwarfs accurately (with the exception of the hottest DAs, which generally contain significant amounts of trace elements). In support of these calibration objectives, we observed a number of hot DA white dwarfs in pointed mode during the initial checkout period. Results will be presented here for WD 0050−332 (GD 659), WD 1620−391 (CD −38° 10980), and WD 1845+019 (BPM 93487). These objects were selected for the initial analysis because the *EUVE* data and the previous EUV observations indicated that these all have pure hydrogen atmospheres. Although we can readily model more complex spectra, including those produced by stratified atmospheres or by atmospheres with significant abundances of trace heavy elements, objects which could be modeled using pure H models were chosen to facilitate the analysis and to provide the most straightforward intercomparison of the *EUVE* results with the results from previous missions.

4. DATA REDUCTION

The data were processed to produce lists of photons that were tagged with arrival time, detector position, and sky coordinates. Nominal count rates were obtained by summing the counts within a given radius from the image centroid and subtracting off a background that was determined from the counts detected within a concentric annulus, then dividing by the exposure time. Two correction factors were then applied to obtain the true count rates. We applied a "dead time" correction to compensate for the finite throughput of the analyzing electronics, and another correction for the losses due to the finite number of available telemetry slots for analyzed events. Scanner observations were always made with the sources not centered in the instrument's fields of view, as necessitated by the filter design. Deep Survey/Spectrometer observations included a combination of on-axis and off-axis pointings. To put the observations on a common basis for comparison, we normalized all count rates to the on-axis values, by dividing by the geometric vignetting factors calculated from raytraces of the instruments, and compared the measurements to models using effective areas which are the nominal on-axis values.

5. DATA ANALYSIS

5.1. *WD 1620−391*

The first spectroscopic/deep survey observation was of WD 1620−391, one of the coolest DA EUV sources, with an optically determined $T_{\rm eff}$ of 24,000 ± 150 K and a log g of 8.08 ± 0.04 based on Balmer line profile fits (Finley, Koester, & Basri 1993b). The corrected *EUVE* count rates and 1 σ errors for each bandpass are listed in Table 1. We analyzed the *EUVE* photometric data using pure H models, varying the temperature and the interstellar column.

Because we have no measurements that include flux longward of the He I ionization edge at 504 Å, we cannot independently measure both the H I and He I columns. However, our measurements shortward of 504 Å are affected by both H I and He I, so we must assume some value for the H I/He I ratio. H I/He I ratios have been published for only two lines of sight to date: G191−B2B, and HZ 43. The values of the H I/He I ratio for G191−B2B were 11–25 (90%; Green, Jelinsky, & Bowyer 1990), and 11.6 ± 1 (1 σ; Kimble et al. 1993a). The HZ 43 result was 7.5–13.5 (1 σ; Kimble et al. 1993b). We assumed an interstellar H I/He I ratio of 10/1, which is consistent with the HZ 43 result. We checked the sensitivity of the results to the assumed H I/He I ratio and found that if a ratio of 12 were adopted, the derived H I columns would change by less than 0.03 dex.

The analysis was performed using a grid of models with temperatures in the range of 23,000 to 26,000 K with a 200 K spacing. Our standard grid is calculated on 0.25 dex intervals in log g. Given the optically determined log g of 8.08, had we used the standard grid value of 8.0, predicted count rates would have been systematically lower by 3% in Lexan/B and by 5% in Al/C. The EUV flux decrease is due to weaker Lyman line blanketing at lower gravity. Thus somewhat higher temperatures would have been required to match the EUV data if the nominal value of 8.0 were used. Therefore, count rates were calculated for both log g = 8.0 and 8.25, and values appropriate for log g = 8.08 were obtained by linear interpolation. Compared to the result obtained with log g set to 8.0, the corrected log g value gave temperatures at the low column limit that were 50 K cooler, while the column upper limit was 0.05 dex higher. We scaled the resulting model fluxes using the published V-magnitude. The model fluxes were then convolved with the ISM attenuation (Rumph, Bowyer, & Vennes 1993) and the instrument effective areas, for which we used the initial calibration reported in Finley et al. (1993a) to obtain predicted count rates.

There are two basic sources of error that affect the accuracy of parameter determinations. We are comparing predicted and measured count rates; the measured count rates are subject to counting statistics, which are of the order of 1% for the cases discussed here. However, the predicted count rates are calculated by convolving model fluxes with the measured effective areas. "Errors" in model fluxes are assumed to be zero, given that aside from systematics, the numerical errors are much less than 1%. The effective areas, though, are subject to significant uncertainty, largely dominated by the 15% absolute error quoted for the efficiencies of the reference photodiodes from the National Institute of Standards and Technology against which the *EUVE* instruments were calibrated. Some additional uncertainty arises in the process of interpolating

© American Astronomical Society • Provided by the NASA Astrophysics Data System

1993ApJ...417..259F

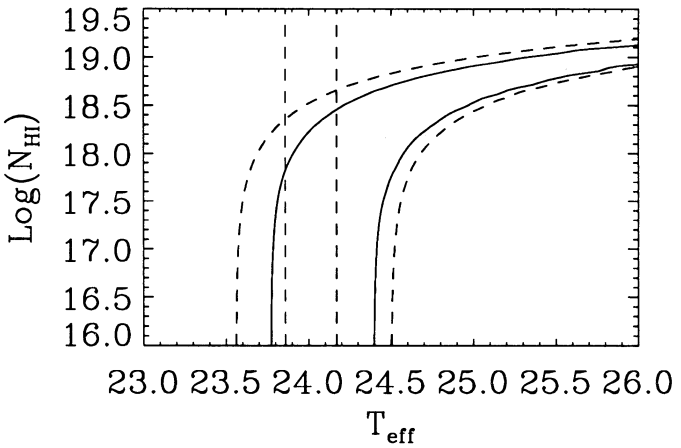

FIG. 1.—68% (1 σ, *solid curve*) and 90% (*dashed curve*) confidence contours obtained from *EUVE* measurements for WD 1620−391, and optical 1 σ temperature limits (*vertical dashed lines*).

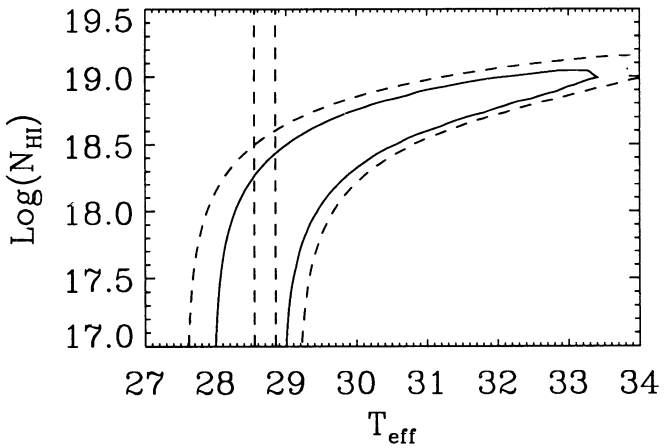

FIG. 2.—*EUVE* and optical results for WD 1845+019; same key as for Fig. 1.

between the wavelengths at which the effective areas were calibrated. (See Finley et al. 1993a for details of the calibration.) Until we perform a detailed cross-comparison between the *EUVE* photometers and the *EUVE* spectrometer for a number of sources to define the effective areas more precisely, we are adopting a conservative overall error of 20% for the photometer effective areas.

Assuming an overall uncertainty in the comparison of predicted and measured count rates of 20%, we calculated the 68% (1 σ) and 90% confidence contours in the $T_{\rm eff}$–$N_{\rm H\,I}$ plane for WD 1620−391, which are shown in Figure 1 along with the 1 σ optical temperature limits. Below log $N_{\rm H\,I} \lesssim 17.5$ the column is seen to have little effect on the predicted Lexan/B and Al/C count rates, given that the temperature changes very little as the H I column is decreased. Note that the inclusion of the Ti/Sb/Ti/Al and Sn upper limits had no appreciable effect on the result. This star is so cool that the intrinsic flux longward of 400 Å is too low for its nondetection in the longer wavelength bandpasses to improve the constraints on the columns. As the column is increased beyond 17.5 dex, the progressively increasing ISM attenuation requires sharply increased temperatures to match the observed count rates. EUV measurements formally allow temperatures in excess of 26,000 K, a result that is clearly inconsistent with the optical determination. The EUV temperature is consistent with our optical value, and the joint optical/EUV constraints give an upper limit for log $N_{\rm H\,I} = 18.45$.

We analyzed the data from the *ROSAT* Position Sensitive Proportional Counter (PSPC) and the *ROSAT* Wide Field Camera (WFC) in a similar manner, using the measured PSPC and WFC count rates from Barstow et al. (1993). The PSPC effective area was provided by T. Fleming (1992, private communication), and the WFC effective areas were obtained from J. Pye (1992, private communication). For very low columns, the PSPC/WFC measurements imply a $T_{\rm eff}$ which is about 25 K lower than that obtained for *EUVE*, an inconsequential difference. In terms of derived columns, the upper limit to $N_{\rm H\,I}$ obtained using the PSPC/WFC data is 18.65 dex.

5.2. *WD 1845+019*

WD 1845+019 was observed with the spectrometers and the Deep Survey instrument. The fit to our optical spectrum for this star yielded an effective temperature of 28,700 ± 150 K, and log $g = 7.87 \pm 0.05$ (Finley et al. 1993b). In this case we used the model grid value of log $g = 7.75$; in this temperature range the log g correction has only a 3% effect on the count rates, which is small compared to the 20% overall uncertainties. The result of our analysis is plotted in Figure 2. Again, the EUV and optical temperatures are consistent, while the combined optical and EUV constraints give a 1 σ upper limit to $N_{\rm H\,I}$ of 18.44 dex.

A somewhat higher Balmer profile temperature was obtained for WD 1845+019 by Bergeron, Saffer, & Liebert (1992, hereafter BSL) using Bergeron's models. Their result was $T_{\rm eff} = 29{,}840$ K, log $g = 7.78$. Assuming that their mean temperature error of 350 K applies in the case of WD 1845+019, their maximum temperature of 30,200 then raises the upper limit for $N_{\rm H\,I}$ obtained from the *EUVE* data to 18.8 dex. We have noted that BSL's Balmer line temperatures are systematically higher than ours, by 2.5%–4%. In their current models, BSL employ the same Stark profiles that are used in our models, and they also calculate the hydrogen level occupation numbers via the Hummer-Mihalas occupation probability formalism. The Hummer-Mihalas treatment, being semi-empirical, does allow some latitude in setting the particular values for the parameters used. BSL have adjusted those parameters in their models to achieve consistent fits to the different lines in the Balmer series for each star. The stars that we have observed optically have tended to be significantly hotter than BSL's sample, and our fits have been consistent for the different Balmer lines for our hotter stars. To check whether our implementation of the Hummer-Mihalas formalism is satisfactory at all temperatures, we have been obtaining data for several cooler DAs (20,000–25,000 K, some in common with BSL), and we will analyze those data and report our results in a future publication. For now, we simply acknowledge the possibility that the effective temperatures may extend somewhat higher than the formal limit allowed by our model fits to the observed Balmer line profiles.

We also analyzed the PSPC/WFC data for this object. The count rates for the WFC were again taken from Barstow et al. (1993), but the corrected PSPC count rate for WD 1845+019 was obtained from T. Fleming (1992, private communication). The comparative result was practically identical to that for WD 1620−391. At very low columns, the PSPC/WFC fits gave a $T_{\rm eff}$ about 150 K lower than for *EUVE*. At the

© American Astronomical Society • Provided by the NASA Astrophysics Data System

1993ApJ...417..259F

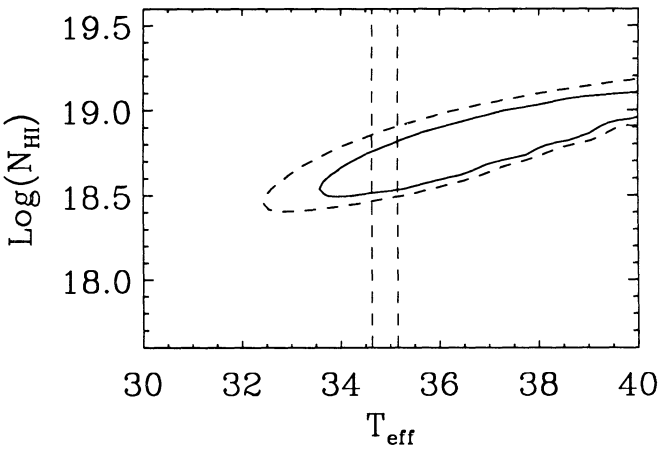

FIG. 3.—*EUVE* and optical results for WD 0050−332; same key as for Fig. 1.

maximum optically determined temperature, the upper limit we obtained for $N_{\rm H\,I}$ was 18.8 dex, 0.36 dex greater than for *EUVE*.

5.3. *WD 0050−332*

WD 0050−332 was observed in pointed mode with the scanner instruments. For this star, our Balmer fit results were $T_{\rm eff} = 34{,}900 \pm 250$ K, log $g = 7.8 \pm 0.08$. Thus, the analysis was performed using log $g = 7.75$ (the gravity corrections to the count rates in this case are at the 1% level). The confidence contours obtained are plotted in Figure 3 with the optical temperature limits. The results are based on measurements for the scanner Lexan/B and Al/C/Ti bandpasses, along with 1 σ upper limits for the scanner Ti/Sb/Ti/Al and Sn bandpasses (see Table 2). For this target, the EUV data alone (including the upper limits) do impose a lower limit to $N_{\rm H\,I}$, which was not the case for WD 1620−391. The long-wavelength bandpass limits provided significant constraints for the hotter of the two objects, because at 35,000 K the intrinsic flux (in photons cm^{-2} s^{-1} Å^{-1}) from a hot DA white dwarf at 400 Å is only a factor of 3 below the peak at 200 Å, whereas at 24,000 K the corresponding drop is a factor of 2500. Including the optical temperature limits, we obtained lower and upper bounds to the $N_{\rm H\,I}$ column of 18.51 and 18.81 dex, respectively.

We also analyzed the PSPC and WFC data for this object, again taking PSPC and WFC count rates from Barstow et al. (1993) and assuming total uncertainties of 20%. In this case, the WFC data alone do not provide a lower limit to the column, while inclusion of the optical temperature limits constrains $N_{\rm H\,I}$ to the range of 18.2–18.95 dex (1 σ).

6. TRACE ELEMENT ABUNDANCES

Fits to the data for all three objects are consistent with pure H atmospheres. While it would be useful to determine upper limits for abundances of any trace elements that might be present, one must first determine which trace elements are appropriate to use. The existence of appreciable amounts of uniformly mixed helium in DA white dwarfs in this temperature range has been ruled out on theoretical grounds (Vennes et al. 1988). The remaining possibilities are that the atmosphere may be stratified or trace metals may be present.

TABLE 2

ISM RESULTS

Name	$l^{\rm II}$	$b^{\rm II}$	$N_{\rm H\,I}$	D (pc)
0050−332.....	299	−84	18.66 ± 0.15	61 ± 17
1620−391.....	341	7	<18.45	12 ± 1.5
1845+019.....	34	2	<18.44	41 ± 7

At present, although some hot DAs are known to contain significant abundances of trace metals, the identities and abundances of those elements are largely unknown. Furthermore, in cases such as these in which the atmosphere is essentially pure H, the photometry cannot distinguish between the existence of stratification and the presence of trace metals, or it may not be sufficiently sensitive to provide significant limits.

For example, for WD 1620−391, Si absorption lines have been detected in *IUE* high-dispersion spectra (Holberg et al. 1985). The radial velocity of the Si lines determined by Holberg et al. was 28.4 ± 4.8 km s^{-1}, which is apparently inconsistent (at the 1 σ level) with Koester's gravitational redshift measurement of 37.9 ± 2.0 km s^{-1} (Koester 1987). However, a photospheric origin for the Si probably cannot be ruled out on the basis of the velocity measurements alone. Assuming a photospheric origin, Vennes et al. (1991) derived abundances of log (Si/H) = −7.1 from the Si II line strengths, or −7.9 based on the Si III lines. We computed models including bound-free Si absorption, with log (Si/H) = −7, to check the effect of Si on the EUV fluxes. We found that Si, at that abundance, had no effect on the *EUVE* Al/C predicted count rate, while the Lexan/B predicted count rate was reduced by only 4% with respect to a pure hydrogen model. Such a small effect is impossible to detect. Furthermore, no significant absorption edges are produced in the model spectrum, implying that unless there are particularly strong absorption lines due to Si which are present in the EUV, low levels of trace Si in DA white dwarfs will be more easily detectable in the far-ultraviolet than in the EUV, contrary to the case for other heavy elements.

Therefore, for elements other than Si in WD 1620−391 and WD 1845+019, we will instead set much tighter limits on departures from pure H using the *EUVE* spectra for these objects. After analyzing a variety of spectra of hot DAs with a range of compositions, we should have a sufficient knowledge of the distribution of trace element abundances to set meaningful limits for the other hot DAs using the photometric data.

7. ISM RESULTS

The characteristics of the targets relevant to the ISM measurements are listed in Table 2. The distances are photometric distances derived by determining the masses and radii from our temperatures and gravities using the CO-core evolutionary models of Wood (1990), and using the relations $f_{5490} = 3.61\ 10^{-9}/10^{0.4m_V}$ and $f_{5490}/H_{5490} = 4\pi(R_*/D)^2$. Here f_{5490} is the isophotal flux for the V-band at 5490 Å, in ergs cm^{-2} s^{-1} Å^{-1}, H_{5490} is the stellar Eddington flux in the same units, and R_* and D are the stellar radius and distance, respectively. The error in the distance is calculated by standard error propagation methods and is dominated by the uncertainty in the determination of log g.

The published astrometric parallax for WD 1620−391 is 0.0673±0.0039 (14.86±0.86 pc, van Altena, Lee, & Hoffleit 1989). To push our photometric distance to the minimum parallax distance would require log $g = 7.8$ at 24,000 K, or $T_{\rm eff} = 29{,}600$ K at log $g = 8.08$. While our formal 1 σ limits for the Balmer line fits for this star are 150 K for $T_{\rm eff}$ and 0.04 for log g, systematic effects of comparable magnitude can

© American Astronomical Society • Provided by the NASA Astrophysics Data System

1993ApJ...417..259F

result from the particular values chosen for the free parameters used in the Hummer-Mihalas formalism for line quenching. Initial tests which we have performed indicate that an appropriate adjustment of those parameters would result in higher temperatures and gravities, and therefore would not explain the apparent parallax discrepancy. A forthcoming parallax measurement from *Hipparcos* will, it is hoped, resolve this discrepancy.

7.1. *WD 1845+019*

The neutral hydrogen column density determination for WD 1845+019 is new; no previous measurement has been published for this object. Column densities have also been measured for two nearby foreground objects using Na I observations: λ Aql, 8° SE of WD 1845+019 and 30 pc distant from the Sun, was stated to have $N_{\rm H\,I} < 18.34$ dex, while ζ Aql, 13° NE of WD 1845+019 at 22 pc has $N_{\rm H\,I} < 18.11$ dex (Welsh et al. 1991). Both Na I upper limits are consistent with our upper limit of 18.44 dex and support the picture that most of the neutral gas is local to the solar neighborhood, and that in this general direction it has quite low neutral hydrogen densities at least between about 20 and 40 pc. While the higher EUV limit of 18.8 dex obtained from the *ROSAT* observation (or from the *EUVE* data if the higher temperature of BSL 1992 is used) is also consistent with low neutral H densities between 20 and 40 pc in the direction of WD 1845+019, the higher limit does allow the possibility of the presence of significant additional neutral material beyond the foreground objects.

Column densities have also been published for δ Aql, which lies 10° E of WD 1845+019, between ζ Aql and λ Aql at a distance of 17 pc. Its proximity to the other two stars and to WD 1845+019 suggests a value for $\log(N_{\rm H\,I})$ much lower than the 19.9 ± 0.2 calculated by de Boer et al. (1986) based on Mg II and other species. The upper limit of 18.72 dex they obtain from Mg I measurements is more consistent with the column densities for the other stars. The remaining nearby star is γ Oph, 15° W of WD 1845+019, at a distance of 38 pc (or about 10 pc from WD 1845+019), for which Frisch & York (1991) estimate $\log(N_{\rm H\,I}) = 19.44$ based on Fe II measurements (a depletion factor of 30 was assumed). While we do not yet know the full extent of the neutral material which is seen in the direction of γ Oph (or its distance from the Sun), our limit for WD 1845+019 indicates that the neutral material extends eastward less than the 10 pc to WD 1845+019.

7.2. *WD 1620−391*

WD 1620−391 was observed by *EXOSAT*. Those observations have been analyzed by a number of authors, whose $N_{\rm H\,I}$ column determinations include the range 18.78–18.95 dex (Paerels et al. 1987), 18.38–19.18 dex (Koester 1989), and 18.7 dex (Vennes 1992). These higher column densities are partially a result of the previous authors taking an effective temperature of around 25,000 K, significantly hotter than our Balmer fit results of 24,000 K. Additionally, our comparisons of *EUVE* and *EXOSAT* count rates for white dwarfs observed by both instruments indicate significant calibration differences between the two instruments' aluminum bandpasses, such that *EXOSAT* column densities are larger than *EUVE* column densities by about 0.3 dex. The source of this difference is currently under investigation. The PSPC and WFC data for WD 1620−391 were analyzed by Barstow et al. (1993), who included the *EXOSAT* Al/P data in order to better constrain $N_{\rm H\,I}$. Their column density of 18.58–18.81 dex is thus subject to the same bias as the other analyses which used only *EXOSAT* data.

Independent column densities have been published for only one other line of sight to a star near WD 1620−391. Based on Mg II measurements, a lower limit for $N_{\rm H\,I}$ of 18.61 dex was obtained for ϵ Sco, which lies at a distance of 19 pc, 7° away (Génova et al. 1986). That measurement, together with our upper limit of 18.45 dex, suggests that a significant amount of neutral material may lie just beyond WD 1620−391.

7.3. *WD 0050−332*

WD 0050−332 was also observed by *EXOSAT*. Published results for $N_{\rm H\,I}$ for this object include 18.7–18.95 dex (Paerels & Heise 1989), 18.95–19.04 dex (Koester 1989), and 18.85 dex (Vennes 1992). These are comparable to our limits of 18.51–18.81 dex; again, the higher *EXOSAT* values reflect the bias due to the *EXOSAT* Al/P bandpass. The result for $N_{\rm H\,I}$ from Barstow et al. (1993) was 18.78–18.81, and again included the *EXOSAT* Al/P measurement for longer wavelength coverage, thus biasing the determination toward somewhat higher column densities. A search of the literature revealed no other published column densities for stars whose line of sight samples the same volume of space as that toward WD 0050−332, the nearest star being 25° away and more than 20 pc distant from WD 0050−332. However, given that our lower limit for WD 0050−332, 18.51 dex, is compatible with the upper limits for our two more nearby targets, this suggests that most of the neutral material along this line of sight is local, and the hydrogen over a substantial fraction of the 60 pc to WD 0050−332 must be largely ionized.

As a check of our column density determinations, we examined the *IUE* spectra of these three stars for indications of possible reddening. All available spectra were co-added and corrected for detector temperature effects and for the *IUE* time-dependent sensitivity degradation using the available *IUE* RDAF procedures. The fluxes were then adjusted with our wavelength-dependent calibration correction based on our Balmer profile temperatures and *IUE* spectra for WD 1620−391, WD 0549+158, and G191−B2B, which was calculated in the same manner as the earlier calibration correction presented in Finley, Basri, & Bowyer (1990). For all three stars discussed, including WD 0050−332, any reddening present is less than 5%, corresponding to $E_{B-V} < 0.005$, implying that $N_{\rm H\,I} < 3 \times 10^{19}$ cm^{-2}, well above our EUV limits.

8. CONCLUSIONS

We find that there is reasonably good agreement between measurements of three hot DA white dwarfs which were made using the *EUVE* Deep Survey and Scanner photometers, and the *ROSAT* PSPC and WFC. Analysis of measurements made by the *ROSAT* PSPC and WFC for the white dwarfs we have investigated give temperatures which are consistent with those obtained using *EUVE* data. *ROSAT* column density measurements, in the cases where only upper limits were obtained, resulted in upper limits of 0.2–0.36 dex larger than those from *EUVE*. In the case of WD 0050−332, for which both instruments obtained measurements, the maximum allowed *ROSAT* column density was larger by 0.14 dex, while the minimum column obtained for *ROSAT* was 0.3 dex lower than for *EUVE*, due to *ROSAT*'s lack of longer wavelength coverage.

In terms of scientific results, the EUV temperatures are consistent with our temperatures determined from Balmer line fits. Assuming pure H compositions, and using our optically deter-

© American Astronomical Society • Provided by the NASA Astrophysics Data System

1993ApJ...417..259F

mined temperature limits, the *EUVE* measurements impose upper limits for the neutral hydrogen column densities toward WD 1620−391 and WD 1845+019 of 18.45 and 18.44 dex, respectively (1 σ). In the case of the more distant WD 0050−332, the 1 σ determination is $N_{\rm H\,I} = 18.66 \pm 0.15$ dex. Our column density determinations confirm many other measurements of low neutral hydrogen column densities in the solar vicinity based on other techniques. Our measurements are consistent with the picture of much of the neutral material seen toward nearby stars being confined to within several parsecs of the Sun. The column measurements for white dwarfs provide data for many lines of sight that cannot be sampled by other measurement techniques, and will help greatly in mapping out the distribution of neutral gas in the solar neighborhood and even beyond 100 pc.

We gratefully acknowledge the literally hundreds of people who have worked for so many years to make *EUVE* a success, including the principal investigators, Roger F. Malina and Stuart Bowyer. We also thank the various members of the data analysis support group who have helped with the data. Lastly, we thank Jim Liebert for helpful comments. D. S. F., P. J., and J. D. are supported by NASA grant NAS5-29298; D. S. F. has additional support from NASA grant NAGW-2478. D. K. is supported by grants from NASA and NSF.

REFERENCES

Barstow, M. A., et al. 1993, MNRAS, submitted
Bergeron, P., Saffer, R. A., & Liebert, J. 1992, 394, 228
Bowyer, S., & Malina, R. F. 1991, in Extreme Ultraviolet Astronomy, ed. R. F. Malina & S. Bowyer (New York: Pergamon), 397
de Boer, K. S., Lenhart, H., van der Hucht, K. A., Kamperman, T. M., Kondo, Y., & Bruhweiler, F. C. 1986, A&A, 157, 119
Finley, D. S., Basri, G., & Bowyer, S. 1990, ApJ, 359, 483
Finley, D. S., Dupuis, J., Paerels, F. B. S., & Koester, D. 1993a, in White Dwarfs: Advances in Observation and Theory, NATO ASI Series, ed. M. A. Barstow (Kluwer: Dordrecht), 201
Finley, D. S., Koester, D., & Basri, G. 1993b, in preparation
Frisch, P. C., & York, D. G. 1991, in Extreme Ultraviolet Astronomy, ed. R. F. Malina & S. Bowyer (New York: Pergamon), 322
Génova, R., Beckman, J. E., Molaro, P., & Vladilo, G. 1986, Adv. Space Res., 6 (2), 53
Green J., Jelinsky P., & Bowyer, S. 1990, ApJ, 359, 499
Holberg, J. B., Wesemael, F., Wegner, G., & Bruhweiler, F. C. 1985, ApJ, 293, 294
Jordan, S., Koester, D., Wulf-Mathies, C., & Brunner, H. 1987, A&A, 185, 253
Kahn, S. M., Wesemael, F., Liebert, J., Raymond, J. C., Steiner, J. E., & Shipman, H. L. 1984, ApJ, 278, 255
Kimble, R. A., et al. 1993a, ApJ, 404, 663
Kimble, R. A., et al. 1993b, ApJ, 408, L41
Koester, D. 1987, ApJ, 322, 852
———. 1989, ApJ, 342, 999
Lampton, M., Margon, B., Paresce, F., Stern, R., & Bowyer, S. 1976, ApJ, 203, L71
Paerels, F. B. S., & Heise, J. 1989, ApJ, 339, 1000
Paerels, F. B. S., Heise, J., Kahn, S. M., & Rogers, R. D. 1987, ApJ, 322, 315
Rumph, T., Bowyer, S., & Vennes, S. 1993, ApJ, submitted
Shipman, H. L. 1979, in IAU Colloq. 53, White Dwarfs and Variable Degenerate Stars, ed. H. M. Van Horn & V. Weidemann (Rochester: Univ. Rochester Press), 86
van Altena, W., Lee, J. T., & Hoffleit, E. D. 1989, General Catalog of Trigonometric Parallaxes (New Haven: Yale Univ. Observatory)
Vennes, S. 1992, ApJ, 390, 590
Vennes, S., Pelletier, C., Fontaine, G., & Wessemael, F. 1988, ApJ, 331, 876
Vennes, S., Thejll, P., & Shipman, H. L. 1991, NATO ASI Series C, vol. 336, White Dwarfs, ed. G. Vauclair & E. Sion (Kluwer: Dordrecht), 235
Welsh, B. Y., Vedder, P. W., Vallerga, J. V., & Craig, N. 1991, ApJ, 381, 462
Wood, M. 1990, Ph.D. thesis, Univ. Texas, Austin

© American Astronomical Society • Provided by the NASA Astrophysics Data System